Structural and photoacoustic studies of mechanically alloyed $Ga_{40}Sb_{38}Se_{22}$ powder

2007 J. Phys.: Condens. Matter 19 186216

(http://iopscience.iop.org/0953-8984/19/18/186216)

IOP PUBLISHING JOURNAL OF PHYSICS: CONDENSED MATTER

J. Phys.: Condens. Matter **19** (2007) 186216 (10pp) doi:10.1088/0953-8984/19/18/186216

Structural and photoacoustic studies of mechanically alloyed $Ga_{40}Sb_{38}Se_{22}$ powder

J C de Lima[1], M Schmitt[2], T A Grandi[1], C E M Campos[1], H Höln[1], S M Souza[1] and D M Trichês[1]

[1] Departamento de Física, Universidade Federal de Santa Catarina, CP 476, 88040-900 Florianópolis, SC, Brazil
[2] Departamento de Engenharia Mecânica, Universidade Federal de Santa Catarina, CP 476, 88040-900 Florianópolis, SC, Brazil

Received 30 November 2006, in final form 5 March 2007
Published 11 April 2007
Online at stacks.iop.org/JPhysCM/19/186216

Abstract

GaSb, GaSe and Ga_2Se_3 alloys were produced by the mechanical alloying technique. Their structural, thermal and optical properties were studied. Some of the results obtained have been reported in some papers referenced here. As an extension to those studies, some mixtures of elemental Ga, Sb and Se powders are now being investigated. Starting from a mixture with nominal $Ga_{62}Sb_{27}Se_{11}$ composition, 9 h of milling resulted in a final product with $Ga_{40}Sb_{38}Se_{22}$ composition and containing nanometric cubic GaSb and an amorphous GaSe phase. Part of this as-milled sample was annealed in order to study the amorphous–crystalline phase transformation. The crystalline cubic GaSb, hexagonal and rhombohedral GaSe phases form the measured x-ray diffraction (XRD) pattern for the annealed sample. The structural and thermal properties of both as-milled and annealed samples were studied by x-ray diffraction, differential scanning calorimetry and photoacoustic spectroscopy (PAS) techniques. We observe that the thermoelastic bending contribution is dominant in the PAS signal for both as-milled and annealed samples. The thermal diffusivity value was calculated for both samples by fitting the PAS signal phase.

1. Introduction

GaSb alloy presents potential applications in semiconductor mid-infrared lasers with emission wavelength in the range of 2–4 μm, which are devices having a variety of military and civil applications such as in infrared imaging sensors, fire detection and for monitoring environmental pollution [1]. Dutta and Bhat [2] compiled an excellent review on the GaSb compound. Unlike the former alloy, Ga_xSe_{1-x} alloys present potential applications in IR detector, MOSFET, solar cell devices [3], optical memory devices [3], electrothermal devices such as solid solution electrodes [4], photovoltaic materials [3, 5] and for optical frequency

conversion in the near to far infrared (1–18 μm) wavelength region. An excellent review has been compiled by Fernelius [6]. Several techniques are used to produce these alloys [1–8].

Since the discovery of the mechanical alloying (MA) technique, it has been used as an alternative technique for synthesizing crystalline, amorphous phases and solid solutions as well as nanostructured materials [9–13]. MA has permitted the production of powders in bulk form and is facilitating the fabrication of massive pieces via consolidation [8].

Recently, nanostructured GaSb [7, 14] and Ga_2Se_3 [8] and amorphous GaSe [15, 16] alloys have been produced by MA in our laboratory. Their structural, thermal and optical properties were studied, and the results were reported in the references above. To the author's knowledge, there are no studies reported in the literature on ternary mixtures of Ga, Sb and Se. Thus, as an extension to those studies, MA has also been applied to investigate some ternary mixtures of Ga, Sb and Se. Potential technological applications for these mixtures need extensive investigations on their physical properties.

In this paper, we report the results obtained for the structural and thermal properties of a mechanically alloyed $Ga_{62}Sb_{27}Se_{11}$ powder. The x-ray diffraction (XRD), differential scanning calorimetry (DSC) and photoacoustic absorption spectroscopy (PAS) techniques were used.

2. Brief theoretical considerations of the photoacoustic absorption spectroscopy applied to semiconductor materials

The thermal diffusivity α, defined as $\alpha = k/\rho c$, where k is the thermal conductivity, ρ the mass density and c the specific heat, is an important parameter to monitor not only for its intrinsic physical interest but also for its use for designing technological devices based on semiconductor materials. Physically, the inverse of α is a measure of the time required to establish thermal equilibrium in a given material. Like the optical absorption coefficient, it is unique for each material. Furthermore, the thermal diffusivity is also known to be extremely dependent upon the effects of compositional and microstructural variables [17] as well as processing conditions (see papers listed in [18]). Thus, the measurement of this parameter is appropriate for following the structural changes promoted by MA processes and annealing effects on the ternary mixture of Ga, Sb and Se investigated.

When the material inside the photoacoustic gas cell absorbs a modulated light beam and generates heat periodically, a PAS signal is created. The dependence of the PAS signal on the optical absorption coefficient and the light-into-heat conversion efficiency allows us to obtain the nonthermal excitation efficiency, the photoinduced energy conversion processes, etc. The PAS signal is directly proportional to the light-into-heat conversion efficiency through the nonradiative processes of the material [19]. For a thermally thick semiconductor sample, there are four processes that may contribute to the PAS signal:

(1) *Intraband nonradiative thermalization*: when the photogenerated electrons relax down to the bottom of the band by creating phonons. The contribution of this process for the PAS signal decreases exponentially with the modulation frequency as $(1/f)\exp(-a\sqrt{f})$, where $a = l_s(\pi/\alpha_s)^{1/2}$, f is the modulation frequency, l_s is the thickness of the sample and α_s is its thermal diffusivity. The PAS signal phase shows a modulation frequency dependence of the type $\Phi_{ph} = \frac{\pi}{2} - af^{1/2}$. When this process is present, it occurs in the low frequency range.

(2) *Nonradiative bulk recombination*: when nonradiative recombination of excess electron–hole pairs after diffusion occurs through a distance $(D\tau)^{1/2}$. The contribution of this process for the PAS signal shows a modulation frequency dependence of the type $f^{-1.5}$. The thermal diffusivity α_s, carrier diffusion coefficient D, surface recombination velocity

v and recombination time τ parameters can be determined by fitting the PAS signal phase to the phase expression given by Pinto Neto [20],

$$\Phi_{\rm ph} = \frac{\pi}{2} + \tan^{-1}\left[\frac{(aD/v)(\omega\tau_{\rm eff}+1)}{(aD/v)(1-\omega\tau_{\rm eff})-1-(\omega\tau_{\rm eff})^2}\right], \tag{1}$$

where $\tau_{\rm eff} = \tau(D/\alpha_{\rm s} - 1)$, and $a = (\pi f/\alpha_{\rm s})^{1/2}$. D is the diffusion coefficient, $l_{\rm s}$ is the thickness of the sample, v is the bulk or surface recombination velocity, $\omega = 2\pi f$, and τ is the relaxation time. When it is present, it occurs in the high frequency range.

(3) *Nonradiative surface recombination*: when nonradiative surface recombination takes place at the sample surface. The contribution of this process for the PAS signal shows a modulation frequency dependence of the type $f^{-1.0}$. Similarly to process (2), the $\alpha_{\rm s}$, D, v and τ parameters can be determined by fitting the PAS signal phase to the phase expression given by Pinto Neto [20]. When it is present, it occurs in the high frequency range after the nonradiative bulk recombination process.

(4) *Thermoelastic bending*: when a temperature gradient generated within the sample across its thickness occurs, there is a contribution of the thermoelastic bending process to the PAS signal. This contribution shows a modulation frequency dependence of the type $f^{-1.0}$. The thermal diffusivity $\alpha_{\rm s}$ can be determined by fitting the PAS signal phase to the expression

$$\Phi_{\rm ph} = \phi_0 + \tan^{-1}\left[\frac{1}{a\sqrt{f}-1}\right], \tag{2}$$

where the constant a is the same as that defined for the intraband nonradiative thermalization process. The PAS signals for the processes (3) and (4) show the same dependence on the modulation frequency. However, the PAS signal phases for each of the processes have different dependences on the modulation frequency. Thus, the analysis of the PAS signal phase permits us to distinguish these processes and determine the $\alpha_{\rm s}$, D, v and τ parameters. In [7], we have shown how each process can be identified through the PAS signal.

3. Experimental procedure

A ternary $Ga_{62}Sb_{27}Se_{11}$ mixture of high purity elemental powders of gallium (Aldrich 99.999%), antimony (Alfa Aesar 99.999%, −200 meshes) and selenium (Alfa Aesar 99.999%, −200 meshes) was sealed together with seven steel balls of 11.0 mm in diameter into a cylindrical steel vial under an argon atmosphere. The ball-to-powder weight ratio was 8:1. The vial was mounted on a SPEX Mixer/mill, model 8000, and milling was performed at room temperature. The structural evolution occurring in the mixture with milling time was followed by recording the x-ray diffraction (XRD) patterns on a Philips X-Pert powder diffractometer, equipped with a graphite monochromator, and using the Cu Kα radiation ($\lambda = 0.154\,06$ nm). After 9 h of milling no more changes were observed, and then the milling process was finished. It was observed that an important quantity of gallium glued onto the vial wall. Then, the as-milled powder was analysed by the energy dispersive x-ray technique in a Shimadzu EDX-700 set-up, and the measured Ga, Sb and Se contents were 40, 38 and 22 at.%, respectively. Low iron contamination (less than 0.50 at.%) was also measured, but due to the small value it will not be considered. Therefore, powder as milled for 9 h will be considered as having a $Ga_{40}Sb_{38}Se_{22}$ composition.

The thermal stability of the as-milled powder was investigated by recording the DSC spectrum from 300 to 890 K, with a heating rate of 10 K min^{-1}, in a TA Instruments 2010 DSC cell, under flowing nitrogen. On the basis of the DSC results, the as-milled powder, in the

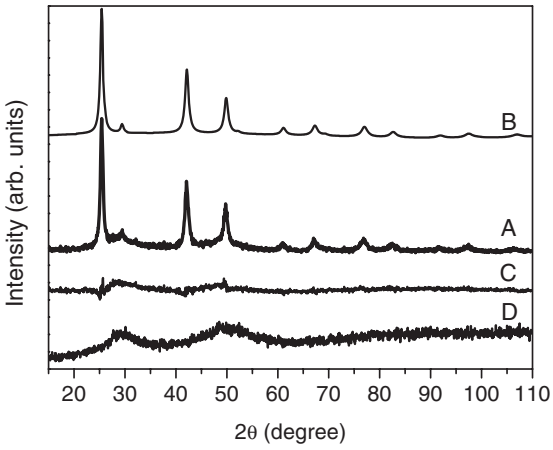

Figure 1. X-ray diffraction patterns: experimental (curve A), simulated (curve B), difference between the experimental and simulated patterns (curve C), and scattering diffuse pattern for the amorphous GaSe alloy as measured by Campos *et al* [15] (curve D).

form of pellets, was sealed in a quartz tube evacuated to about 10^{-3} Torr and annealed at 653 and 798 K for 360 and 210 min, respectively; this was followed by air cooling. The annealed powder was again analysed via the XRD technique.

The PAS measurements were performed in a home-built open photoacoustic cell (OPC) configuration. The OPC configuration consists of a 250 W quartz–tungsten–halogen (QTH) lamp, which has the current stabilized by a Bentham 605 power supply, after being heat filtered by a water lens, and is mechanically chopped by a Perkin–Elmer light chopper, model 197, and focused onto the sample. The sample is mounted directly onto the front sound inlet of an electret microphone [18]. The output voltage from the microphone is connected to a lock-in amplifier, which is linked to a PC computer to record the PAS signal amplitude and phase as a function of the modulation frequency. The as-milled and annealed $Ga_{40}Sb_{38}Se_{22}$ samples for PAS measurements were prepared by compressing the powders at the same pressure to form tiny circular pellets of 10 mm in diameter, with thickness of 545 and 550 μm, respectively.

4. Results and discussion

4.1. XRD and DSC measurements

Figure 1 shows the measured XRD pattern (curve A) of the $Ga_{40}Sb_{38}Se_{22}$ sample milled for 9 h, and it is quite different from those corresponding to the elemental Ga, Sb and Se elements. From this figure one can see that the milling process promoted the nucleation of a crystalline and an amorphous phase. The presence of the latter is clearly evidenced by the discrepancies located at about $2\theta = 28°$ and 48°. The crystalline XRD pattern was compared with those given in the JCPDS database [21] for the GaSb phase and there was found a good agreement with that for the cubic phase (card 07-0215). This XRD pattern was also compared with that reported by us for the single cubic GaSb phase prepared by MA [7, 14], and there was found an excellent agreement there as well. The amount of amorphous phase present in the as-milled $Ga_{40}Sb_{38}Se_{22}$ sample was calculated by using the Ruland method [22] and the value found was $\approx$42%.

The XRD pattern corresponding to the GaSb phase was simulated using the Rietveld structural refinement procedure [23] through the code DBWS 9807. The structural model for this phase was taken from the TAPP 2.2 software [24], and the best fitting was reached by considering the lattice parameter $a = 0.606\,82$ nm ($a = 0.609\,59$ nm). The value shown in the brackets is that given in the TAPP 2.2 software for this phase. The simulated XRD pattern (curve B) is

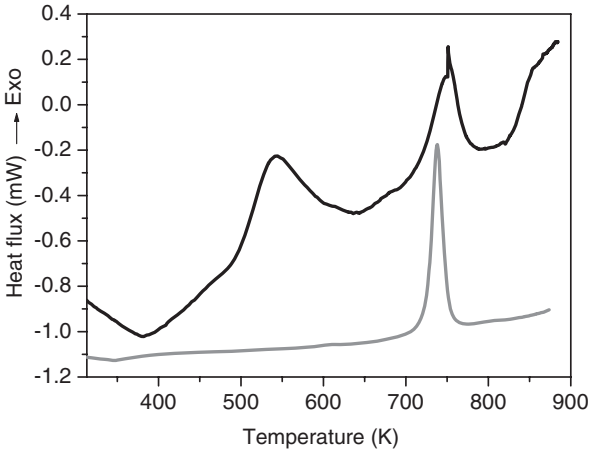

Figure 2. DSC spectrum of $Ga_{40}Sb_{38}Se_{22}$ sample milled for 9 h. The measurement was done with a heating rate of 10 K min^{-1}.

shown in figure 1, and an excellent agreement between the experimental and simulated patterns is observed. In this figure there is also shown the difference between them (curve C), which has the form of a diffuse scattering, characteristic of an amorphous phase. This difference shows two haloes located at about $2\theta = 28°$ and 48°. In order to identify this amorphous phase, the curve D depicts the diffuse scattering pattern for the amorphous GaSe phase measured by Campos *et al* [15]. A good agreement between them is observed, suggesting that the amorphous phase present in the as-milled $Ga_{40}Sb_{38}Se_{22}$ sample has a composition around the equiatomic one. This suspicion will be confirmed through annealing and it will be discussed later.

All the peaks on the XRD pattern for the GaSb phase are enlarged, indicating a nanometric structure. The nanometric structure is formed by crystallites having dimensions of a few nanometres (from 2 up to 100 nm) [25]. The mean size of the crystallites can be satisfactorily estimated from the simulated XRD pattern taking into account the line broadening caused by both crystallite size and strain, through the relationship [26]

$$\left(\frac{\beta_t \cos\theta}{K\lambda}\right)^2 = \frac{1}{d^2} + \sigma_p^2 \left(\frac{\sin\theta}{K\lambda}\right)^2, \tag{3}$$

where θ is the diffraction angle, λ is the x-ray wavelength, β_t is the total broadening measured at the peak's full width at half-maximum (FWHM) in radians, d is the crystallite size, σ_p is the strain, and K is a constant dependent on the measuring conditions and on the definition of β_t and d (here it was assumed to be 0.91 as usual in the Scherrer formula). Graphical linearization of the relationship above, i.e., plotting of $\beta_t^2 \cos^2\theta/\lambda^2$ versus $\sin^2\theta/\lambda^2$, yields the mean crystallite size free from strain effects from the values of the intercept of the straight line obtained. The strain is obtained from the slope of the linearized graph. The code DBWS 9807 generates the β_t and 2θ positions for all the simulated peaks, and considering these values in expression (2), we find $d \approx 12.4$ nm and $\sigma_p \approx 2.90\%$.

Figure 2 shows the measured DSC curve of the $Ga_{40}Sb_{38}Se_{22}$ sample milled for 9 h. We can see a broad endothermic band located in the 315–490 K range and two exothermic peaks whose maxima occur at about 548 and 750 K. There is also a broad exothermic band starting at about 800 K, which is incomplete due to limitations of the Al pans used in the DSC cell. In order to make the interpretation of the DSC curve, the result for the amorphous GaSe phase (grey line curve) as measured by Campos *et al* [15] is also depicted in this figure. The melting point of the Sb_2Se_3 compound is $T_m = 863$ K, while those of some selenium oxides are: SeO_2 ($T_m = 589$ K), SeO_3 ($T_m = 667$ K), Se_2O_5 ($T_m = 497$ K). The measured DSC curve does

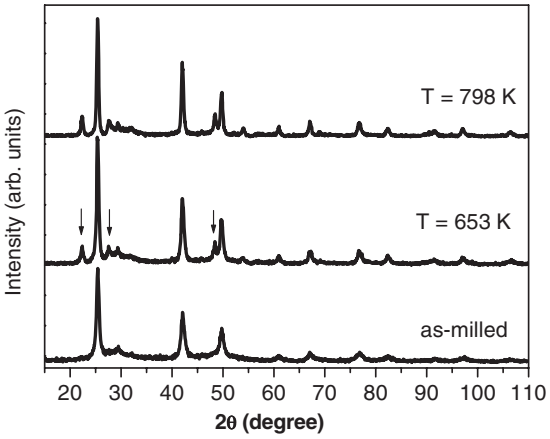

Figure 3. X-ray diffraction patterns: as-milled (bottom), annealed at 653 K (middle) and annealed at 798 K (top).

not show any endothermic peak associated with melting. This result indicates the absence of unreacted Se (T_m = 494 K), antimony (T_m = 903.78 K) powders, selenium oxides and Sb_2Se_3 compound, even in small quantities, in the as-milled sample. It corroborates the results obtained by XRD analysis for this sample. The endothermic band is associated with elimination of water molecules coming from the wet and that are located at the surface particles. This endothermic peak agrees with that reported in [7] for the cubic GaSb phase prepared by MA. The exothermic peak at 750 K agrees reasonably with the temperature for the amorphous–crystalline transformation observed by Campos *et al* [15]. The interpretation of the exothermic peak located at about 548 K and of incomplete broad exothermic band will be done later. The enthalpy changes for exothermic peaks at about 548 and 750 K were calculated and the values found were 14.5 and 7.8 J g^{-1}, respectively.

On the basis of the DSC curve, a small amount of the $Ga_{40}Sb_{38}Se_{22}$ sample was annealed at 653 K for 360 min and at 798 K for 210 min, and this was followed by air cooling. Their XRD patterns were measured and they are shown in figure 3. The XRD pattern of the as-milled sample is also shown in this figure to facilitate its interpretation. After annealing at 653 and 798 K, the cubic GaSb phase remains stable. However, after annealing at 653 K, new peaks (marked by the arrows) arose and they remained after the second annealing at 798 K. It is interesting to note that the annealing at 798 K was not sufficient to eliminate completely the amorphous phase. According to the Ga–Se phase diagram [27], two different phases of closely related crystal structures exist in the equiatomic region: a hexagonal phase, with composition between 48 and <51 at.% Se, and a rhombohedral phase with composition between 52 and 53.5 at.% Se. A narrow two-phase field separates these phases. These new peaks show a good agreement with the XRD patterns given in the JCPDS database for the rhombohedral and hexagonal GaSe compounds (card Nos 81-1971 and 71-0375). On the basis of these results, the exothermic peaks located at about 548 and 750 K on the DSC curve can be attributed to the crystallization of amorphous GaSe phases, which have very close chemical compositions and very different crystallization temperatures.

The incomplete broad exothermic band can be analysed by considering the obtained XRD results for the annealed sample. According to Vigil-Galán *et al* [28], the formation of native oxides in as-grown GaSb samples in oxygen atmosphere obeys the chemical reaction $2GaSb + 3O_2 \rightarrow Ga_2O_3 + Sb_2O_3$. The only stable phases that can exist in thermodynamic equilibrium with GaSb are Ga_2O_3 and elemental antimony. Thus, the Sb_2O_3 oxide should react with the GaSb sample to produce more Ga_2O_3 and free Sb through the chemical reaction

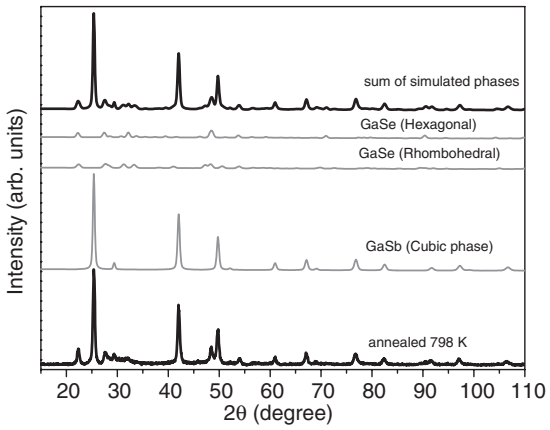

Figure 4. X-ray diffraction pattern of $Ga_{40}Sb_{38}Se_{22}$ sample annealed at 798 K (bottom), simulated cubic GaSb, rhombohedral and hexagonal GaSe phases and the sum of all the three simulated patterns (top).

$Sb_2O_3 + 2GaSb \rightarrow Ga_2O_3 + 4Sb$. We experimentally confirmed these predictions [7]. The XRD pattern depicted in figure 3 does not show Ga_2O_3 and/or pure Sb. Thus, we have attributed the incomplete broad exothermic band shown in the DSC curve (see figure 2) to the expected specific heat behaviour with increasing temperature.

Using the Rietveld structural refinement procedure also simulated the XRD pattern showed in figure 3. Besides the crystallographic data for the cubic GaSb phase used previously, those given in the ICSD Database [29] for the GaSe rhombohedral (ICSD code No 73388) and hexagonal (ICSD code No 2002) phases were considered, and the best fit was reached when the rhombohedral and hexagonal GaSe phases were considered together with the GaSb one. The refined lattice parameters are $a = b = 0.376\,34$ nm (0.373 nm) and $c = 2.380\,57$ nm (2.386 nm) for the rhombohedral GaSe, $a = b = 0.376\,84$ nm (0.3755 nm) and $c = 3.193\,66$ nm (3.199 nm) for the hexagonal GaSe, and $a = b = c = 0.607\,27$ nm for the cubic GaSb phase. The values in the brackets are those given in the ICSD Database. The simulated patterns (middle grey solid and top black lines) are shown in figure 4. The code DBWS 9807 calculates the relative percentage of amounts of phases, and from a best fit the calculated amounts are 62.84%, 19.95% and 17.21% for the GaSb, GaSe (rhombohedral) and GaSe (hexagonal), respectively. These values are slightly overestimated due to the amount of the amorphous phase still present after annealing. It is interesting to note that the sum of relative percentage GaSe amounts (37.16%) is near to the one found previously for the amorphous phase (42%).

After annealing at 798 K, the mean sizes of the crystallites and strain for the GaSb phase were calculated, and the values found are $d \approx 15$ nm and $\sigma_p \approx 1.38\%$. For the GaSe phases, these quantities were not evaluated due the low intensity of the peaks on the XRD pattern. The increasing of the mean crystallite size with annealing, as well as the reduction of the strain, is associated with partial elimination of the interfacial component and strains in the crystalline one. As a consequence, an improvement in the crystallinity of the sample is observed.

4.2. Determination of thermal diffusivity parameter from the PAS measurements

The characteristic frequency $f_c = \frac{\alpha_s}{\pi l_s^2}$ is the modulation frequency making the transition from the thermally thin regime ($f < f_c$) to the thermally thick regime ($f > f_c$). Marin *et al* [30] reported the thermal diffusivity value of 0.24 $cm^2\ s^{-1}$ for the GaSb compound, and more recently, we reported [7] the values of 0.245 and 0.216 $cm^2\ s^{-1}$ for as-milled and annealed GaSb samples, respectively. Since the thicknesses of our samples are 545 and 550 μm, the modulation frequency was varied from 10 to 270 Hz in order to achieve the thermally thick regime.

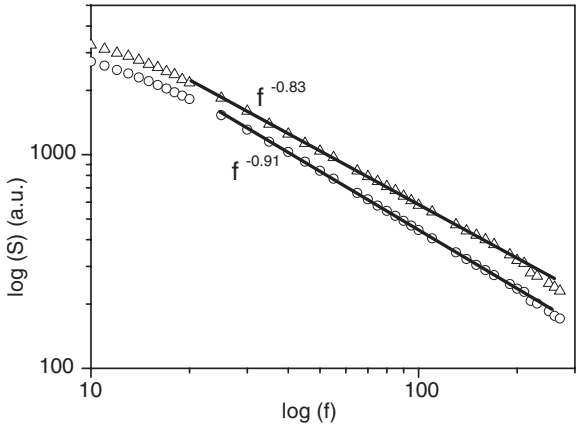

Figure 5. PAS signal amplitude versus modulation frequency for the as-milled (open circle line) and annealed (open triangle line) $Ga_{40}Sb_{38}Se_{22}$ samples. The solid lines correspond to the modulation frequency region where the thermoelastic bending process is the dominant contribution for the PAS signal amplitude.

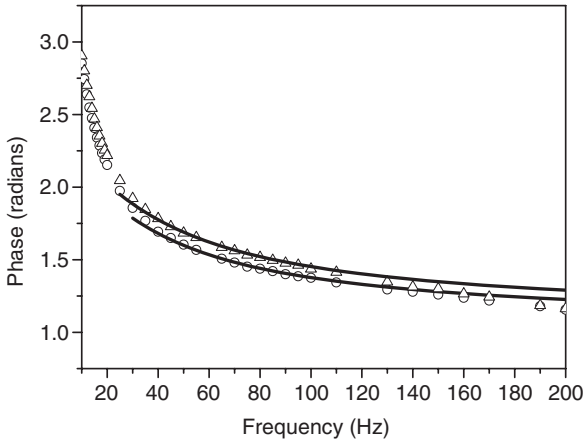

Figure 6. PAS signal phase versus modulation frequency for the as-milled (open circle line) and annealed (open triangle line) $Ga_{40}Sb_{38}Se_{22}$ samples. The solid lines correspond to the best fit of the experimental data using equation (2).

Figures 5 and 6 show the PAS signal amplitude and phase for the as-milled (open circle line) and annealed (open triangle line) samples, respectively. After annealing, the signal amplitude increased by 19%, while the phase increased by 4.4% between 35 and 100 Hz. Using the procedure described in [7], it was observed that the intraband nonradiative thermalization and nonradiative bulk recombination processes do not contribute to the PAS signal amplitude. As depicted in figure 5, the PAS signal amplitude for both as-milled and annealed samples shows a dependence of the type $f^{-0.9}$ on the modulation frequency, which is characteristic of the nonradiative surface recombination, thermoelastic bending process or thermal dilation [31]. The thermal dilation process produces a signal whose phase is independent of the modulation frequency and equal to $-90°$, a fact that is not observed in figure 6. Recently, we reported the values for the thermal diffusivity α_s, D, v, and τ for as-milled and annealed GaSb samples prepared by MA [7]. These values were unsuccessfully used in the phase expression given

by Pinto Neto [20], reproduced as expression (1), for the nonradiative surface recombination process. The fit was applied in the Φ_{ph} (in radians) versus f graph only considering the phase and modulation frequency data corresponding to the straight line shown in figure 5. Thus, the contribution of the nonradiative surface recombination process to the PAS signal amplitude was also discarded. On the other hand, the expression for the phase corresponding to the thermoelastic bending process, reproduced as expression (2), was successfully fitted to this region of the Φ_{ph} (in radians) versus f plot. For as-milled and annealed samples, the best fits were reached for $\alpha_s = 0.1850$ and 0.1985 cm^2 s^{-1} values, respectively, and they are shown as solid lines in figure 6. The thermal diffusivity values of the amorphous and crystalline phases differ by one up two orders of magnitude. A slight increase in the α value for the annealed sample is observed. We have attributed this increase to the improvement in the crystallinity of the GaSb phase and GaSe amorphous–crystallization transformation. However, these values are smaller than those previously reported by us for as-milled and annealed GaSb samples [7]. We reported thermal diffusivity values of 0.082 and 0.097 cm^2 s^{-1} for as-milled and annealed Ga_2Se_3 samples [8]. These values differ by one order of magnitude from that reported by Barbu *et al* [32] for GaSe:B single crystals ($\alpha = 0.004\,13$ cm^2 s^{-1}).

In order to understand the reduction in the thermal diffusivity value of $Ga_{40}Sb_{38}Se_{22}$ samples when compared with those reported in [7], the microstructure of ternary as-milled and annealed samples must be analysed. The microstructure of the as-milled sample is formed by nanometric cubic GaSb and amorphous GaSe phases, and the relative amounts are similar. We believe that the amorphous GaSe phase is located among GaSb particles and that it is responsible by reduction in the thermal diffusivity value. Due to chemical disorder present in the amorphous GaSe phase empty spaces (like pores) may appear, originating temperature gradients inside the sample. These temperature gradients are responsible for the predominance of the thermoelastic bending process in the PAS signal amplitude and phase. Cubic GaSb, hexagonal and rhombohedral GaSe phases and a remaining amorphous GaSe one form the microstructure of the annealed sample. The coexistence of the three crystalline phases may induce lattice mismatch, originating empty spaces (like pores), a fact that favours the appearance of a temperature gradient inside the sample. Beyond this, the remaining amorphous GaSe phase may be located among particles of these crystalline phases. We believe that the lattice mismatch and/or remaining amorphous GaSe phase are responsible for the reduction in the thermal diffusivity value. The small difference between the thermal diffusivity values for the ternary as-milled and annealed samples suggests that the amorphous phase and lattice mismatch have similar effects on the propagation of thermal waves in the samples.

5. Conclusions

The main conclusions drawn from this study are:

(1) The milling of a $Ga_{62}Sb_{27}Se_{11}$ mixture for 9 h resulted in a final product with $Ga_{40}Sb_{38}Se_{22}$ composition and containing the nanometric cubic GaSb phase and an amorphous GaSe one.
(2) Annealing of the as-milled sample resulted in the amorphous GaSe phase crystallization in the rhombohedral and hexagonal GaSe phases. It promoted also the grain growth of the cubic GaSb phase from 12.4 to 15 nm, and reduction in strains as well.
(3) The thermal diffusivity value for the annealed sample is slightly greater than that measured for the as-milled one. This increment is attributed to the improvement in the crystallinity of the cubic GaSb sample and the crystallization of the amorphous GaSe phase.
(4) The reduction of the thermal diffusivity value of the ternary as-milled $Ga_{40}Sb_{38}Se_{22}$ sample when compared with value previously reported for GaSb compounds produced by MA

was attributed to the large quantity of amorphous GaSe phase present in this as-milled sample, while the reduction in this parameter observed for the annealed $Ga_{40}Sb_{38}Se_{22}$ sample was mainly attributed to the lattice mismatch among the cubic GaSb, hexagonal and rhombohedral GaSe phases and the presence of a remaining amorphous GaSe phase.

Acknowledgments

The authors thank the Brazilian agencies CNPq, FINEP and FAPESC for material and financial support. They thank Dr P B Prates for the XRD measurements and Dr N S Branco for carefully reading the manuscript.

References

[1] Mourad C, Gianardi D, Malloy K J and Kaspi R 2000 *J. Appl. Phys.* **88** 5543
[2] Dutta P S and Bhat H L 1997 *J. Appl. Phys.* **81** 5821
[3] Gupta P and Bhatnagar P K 2000 *Mater. Charact.* **45** 167
[4] Afifi M A, Bekheet A E, El-Shair H T and Zedan I T 2003 *Physica* B **325** 308
[5] Dai Z R and Ohuchi F S 1998 *Appl. Phys. Lett.* **73** 966
[6] Fernelius N C 1994 *Prog. Cryst. Growth Charact.* **28** 275
[7] de Lima J C, Schmitt M, Souza S M, Almeida T O, Jerônimo A R, Triches D M, Grandi T A and Campos C E M 2007 *J. Alloys Compounds* at press
[8] Souza S M, Campos C E M, de Lima J C, Grandi T A and Pizani P S 2006 *Solid State Commun.* **139** 70
[9] de Lima J C, Trichês D M, dos Santos V H F and Grandi T A 1999 *J. Alloys Compounds* **282** 258
[10] Weeber A W and Bakker H 1988 *Physica* B **115** 93
[11] Mukhopadhyay D K, Suryanarayana C and Froes F H 1994 *Scr. Metall. Mater.* **30** 133
[12] Yavari A R, Desré P J and Benameur T 1992 *Phys. Rev. Lett.* **68** 2235
[13] Gutmanas E Y 1989 *Proc. DGM Conf. on New Materials by Mechanical Alloying Techniques* ed E Arzt and L Schultz (Oberursel: DGM Informationsgesellschaft) p 129
[14] Campos C E M, de Lima J C, Grandi T A, Schmitt M and Pizani P S 2006 *J. Phys.: Condens. Matter* **18** 8613
[15] Campos C E M, de Lima J C, Grandi T A, Machado K D and Pizani P S 2003 *Solid State Commun.* **126** 611
[16] Machado K D, Jóvari P, de Lima J C, Campos C E M and Grandi T A 2004 *J. Phys.: Condens. Matter* **16** 581
[17] Ziegler G and Hasselman D P H 1981 *J. Mater. Sci.* **16** 495
[18] de Lima J C, Cella N, Miranda L C M, Chying An C, Franzan A H and Leite N F 1992 *Phys. Rev.* B **46** 14186
[19] Pao Y (ed) 1977 *Optoacoustic Spectroscopy and Detection* (New York: Academic) p 425
[20] Pinto Neto A, Vargas H, Leite N F and Miranda L C M 1990 *Phys. Rev.* B **41** 9971
[21] 2000 Joint Committee on Powder Diffraction Standards (JCPDS), Philadelphia
[22] Ruland W 1961 *Acta Crystallogr.* **14** 1180
[23] Rietveld H M 1969 *J. Appl. Crystallogr.* **2** 65
[24] *TAPP* version 2.2, ES Microwave Inc., Wade Court, Hamilton, OH
[25] Gleiter H 1989 *Prog. Mater. Sci.* **33** 223
[26] Strnad Z 1986 Glass–ceramic materials *Glass Science and Technology* vol 8 (Amsterdam: Elsevier) p 161
[27] Hansen M and Anderko K 1991 *Constitution of Binary Alloys* 2nd edn (New York: Genium/McGraw-Hill)
[28] Vigil-Galán O, Ximello-Quiebras J N, Aguilar-Hernández J, Contreras-Puente G, Cruz-Orea A, Mendonza-Álvarez J G, Cardona-Bedoya J A, Ruiz C M and Bermúdez V 2006 *Semicond. Sci. Technol.* **21** 76
[29] 1995 *Inorganic Crystal Structure Database (ICSD),* Gmelin-Institut für Anorganische Chemie and Fachinformationszentrum, FIZ Karlsruhe
[30] Marin E, Riech I, Diaz P, Alvarado-Gil J J, Baquero R, Mendoza-Alvarez J G, Vargas H, Cruz-Orea A and Vargas M 1998 *J. Appl. Phys.* **83** 454
Marin E, Riech I, Diaz P, Alvarado-Gil J J, Baquero R, Mendoza-Alvarez J G, Vargas H, Cruz-Orea A and Vargas M 1998 *J. Appl. Phys.* **83** 2604
[31] Rousset G, Lepoutre F and Bertrand L 1983 *J. Appl. Phys.* **54** 2383
[32] Barbu A, Cristea Gh, Bratu I, Munshinskii V P and Bobis I 1997 *J. Mol. Struct.* **410/411** 259